DELPHI Collaboration

DELPHI 2001-021 CONF 462
01 March, 2001

Measurement of tau polarisation at LEP2

Igor Boyko
JINR, Dubna, Russia

Abstract

This note describes the first measurement of polarisation of tau leptons produced in reaction $e^+e^- \to \tau^+\tau^-(\gamma)$ at LEP energies above the Z resonance. One prong hadronic tau decays have been selected from non-radiative sample of tau pairs. The polarisation was extracted from distribution of angles characterising tau decays and subsequent decays of hadronic resonances. The analysis of 1997-1999 LEP data has given a result compatible with the Standard Model prediction.

Results prepared for Winter Conferences 2001

1 Introduction

This note describes the measurement of polarisation of tau leptons produced in reaction $e^+e^- \to \tau^+\tau^-(\gamma)$ at LEP energies around 200 GeV. This analysis is a modification of the LEP1 measurement of tau polarisation through its one-prong hadronic decays [1]. The polarisation value was extracted from data using the same technique as at LEP1, while the event selection was significantly modified to preserve high selection efficiency and a modest background level. The systematic uncertainties were carefully analysed. Given the very small tau pair cross-section at LEP2, the total error is dominated by the event statistics.

2 Event selection

This section describes the preselection of tau pairs and the cuts used for the tau hadronic decay selection. The selection cuts are illustrated by plots which the following convention (unless other is specified): points with error bars are real data (1997-99), white histogram is Monte-Carlo simulation, black histogram is contribution of non-tau background, and gray histogram is contribution of leptonic and multi-prong tau decays.

The analysis was based on the event sample selected for the measurement of tau pair cross-section and forward-backward asymmetry. The selection procedure is described in details in [2]. The actual annihilation energy, $\sqrt{s'}$ (see [2] for details), was required to be more than 90% of the LEP centre-of-mass energy. With this cut 737 non-radiative tau pair candidates were selected from the data collected by DELPHI in 1997-1999 (about 430 pb^{-1} integrated luminosity). The non-tau background level of this sample was about 12%. No special attempt was done to further reduce this background. However, since the non-tau background is dominated by leptonic final states, its level was significantly reduced by selection of tau hadronic decay.

The selected tau pair events were divided into two jets using the jet clustering algorithm (see [2]) and each jet was considered as a tau decay candidate. To ensure a good performance of electromagnetic calorimetry the jet highest momentum ("leading") track had to lie in the DELPHI barrel region (polar angles $42^0 < \Theta < 88.3^0$ or $91.7^0 < \Theta < 138^0$). Tracks pointing to the boundaries between modules of the DELPHI electromagnetic calorimeter (HPC) were rejected.

For each jet the jet invariant mass M_{INV} was calculated using the leading track (assuming it was a pion) and all the photons reconstructed in a 30^0 cone around the leading track Only jets with invariant mass less than 2 GeV/c^2 were selected for the analysis.

The following cuts were then applied to each jet to select one-prong hadronic tau decays:

- To reject multi-prong tau decays while keeping gamma conversions the number of tracks with vertex detector (VD) hits was required to be exactly 1.
- To reject low momentum electrons the dE/dx pull for pion hypothesis was required to be less than +2 (i.e. dE/dx was less than 2 standard deviations from the value expected for a pion). The distribution of the dE/dx pull is presented in Fig.1 for three ranges of track momentum.

- To reject electrons of higher momentum the following "OR" condition was applied: either the HPC energy associated to the charged track was less than 10 GeV, or the hadron calorimeter (HCAL) energy beyond its first layer associated to the charged track was more than 0.5 GeV. The distribution of the HPC energy is presented in Fig.2.

The performance of the combined HPC/HCAL cut is illustrated in Fig.3 which shows the momentum dependence of selection efficiency for each condition and for the "OR" of them. The overall performance of electron background rejection is presented in Fig.4. The plot shows momentum dependence of $\tau \to e\nu\nu$ contamination before electron rejection (white histogram), after dE/dx cut (gray histogram) and after dE/dx and HPC/HCAL cut (black histogram). The largest residual background is observed in the intermediate region around 10 GeV/c momentum which is too high for efficient dE/dx separation but too low for reliable electron identification with HPC.

- The muons were rejected asking that there was no muon chamber hit associated to the charged track.

This cut was sufficient for the jet invariant mass region $M_{INV} > 0.3\ GeV/c^2$. However in the region of lower invariant masses the muon background was still too high. To further reduce it, the following cut was applied only to the events with $M_{INV} < 0.3\ GeV/c^2$:

- The average HCAL energy per layer associated to the leading track ($AVHC$) had to be not in the range $0.5\ GeV < AVHC < 1.5\ GeV$. which is expected for a MIP. Fig.5 presents the distribution of $AVHC$ variable for tau hadronic decays. The distribution of the same variable for a test sample of tau decays to muons selected with muon chambers is presented in Fig.6.

After the selection described above about 450 one-prong hadronic tau decays have been selected from 1997-99 data. The selection efficiency is shown in Fig. 7 as a function of the track momentum. The overall efficiency (within the HPC angular acceptance) was 76.9% (82% for pions, 77% for rhos and 70% for a_1's). The momentum distribution for all the selected events is shown in Fig. 8.

The residual background from non-tau pair processes was 4.5%. Largest contributions were from $\gamma\gamma \to \tau\tau$ process and from W pairs. The relative uncertainty of the external background level was about 20-25%. The internal background was 6.4%, with 1.1% coming from $\tau \to e\nu\nu$, 1.8% from $\tau \to \mu\nu\nu$, and the remaining background was from multi-prong tau hadronic decays.

3 Extraction of polarisation

Similar to LEP1 analysis [1] the tau polarisation value was extracted by simultaneous fit of Monte-Carlo to data distributions in several regions of jet invariant mass. The distribution of invariant mass for all the selected events is shown in Fig. 9. The events were separated into three samples according to the reconstructed jet invariant mass M_{INV}: $M_{INV} < 0.3\ GeV/c^2$ (dominated by $\tau \to \pi\nu$ decays), $0.3\ GeV/c^2 < M_{INV} < 0.8\ GeV/c^2$ (dominated by rhos) and $0.8\ GeV/c^2 < M_{INV} < 2.0\ GeV/c^2$ (mixture of rhos and a_1's).

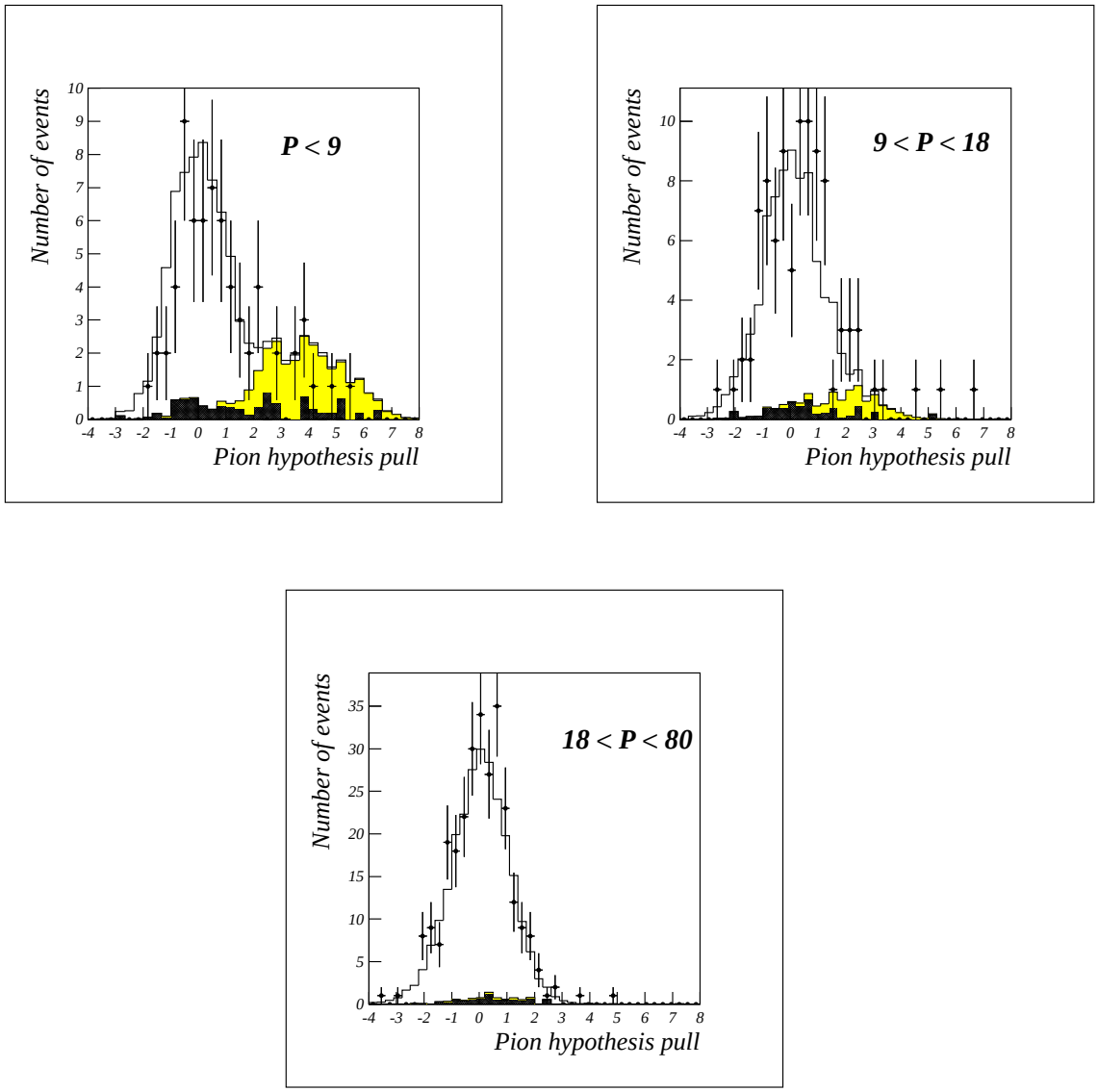

Figure 1: Distribution of dE/dx pull for the events selected for polarisation measurement in different momentum regions: $p < 9\ GeV/c$ (upper left), $9\ GeV/cp < 18\ GeV/c$ (upper right), and $p > 18\ GeV/c$ (lower). The value of selection cut is 2.0

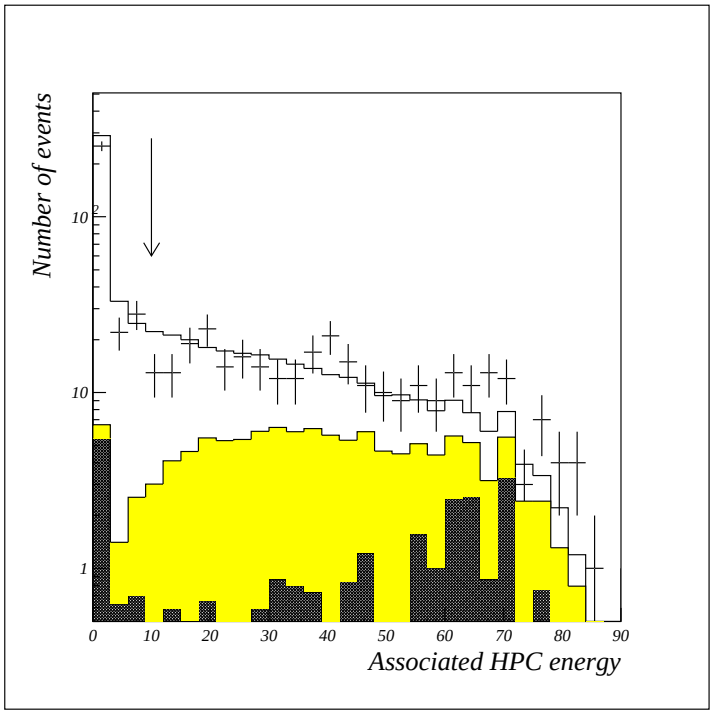

Figure 2: Distribution of HPC energy associated to the track for the events selected for polarisation measurement. The cut value is shown by an arrow.

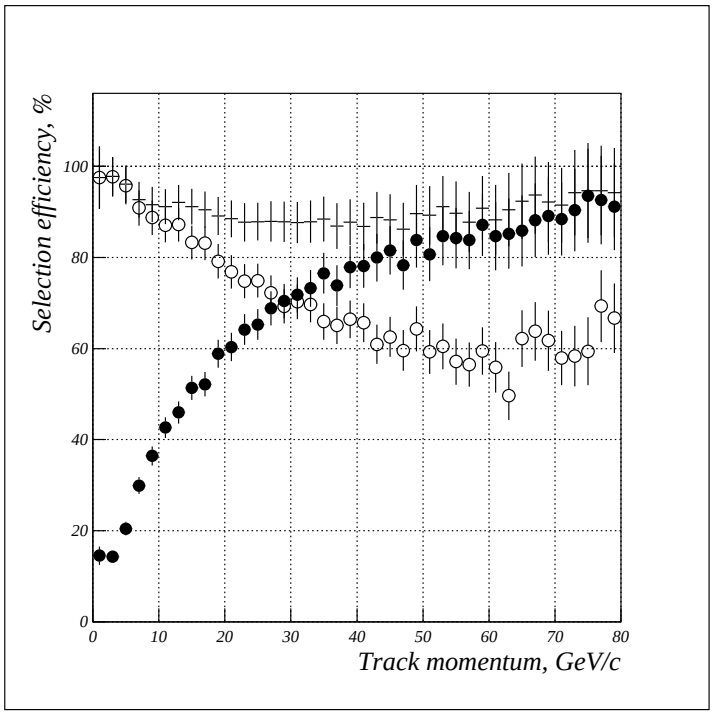

Figure 3: Momentum dependence of selection efficiency of the cut on HPC associated energy (open circles), HCAL associated energy (filled circles) and of the "OR" of the two (crosses). All efficiencies are estimated from Monte-Carlo.

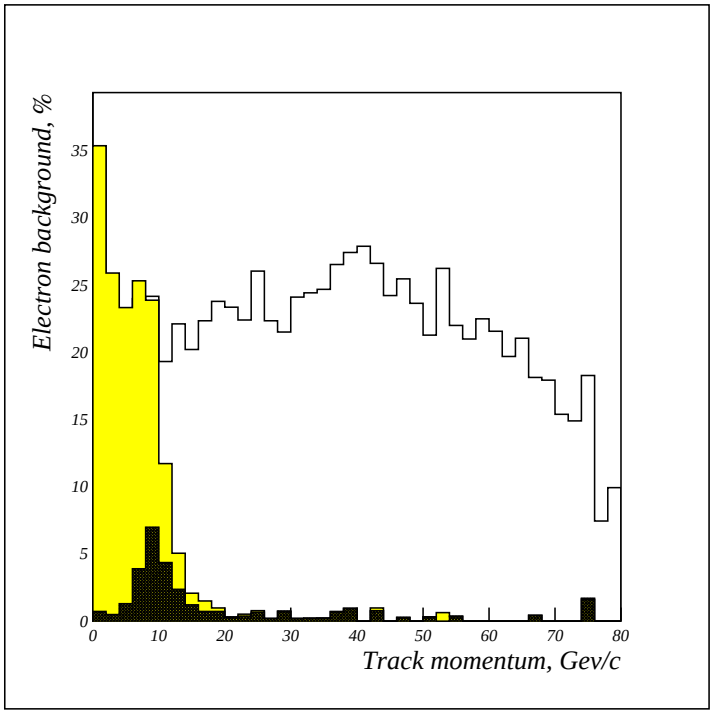

Figure 4: The momentum dependence of electron background level before electron rejection (white), after HPC/HCAL cut (gray) and after dE/dx and HPC/HCAL cut (black). The background was estimated from simulation.

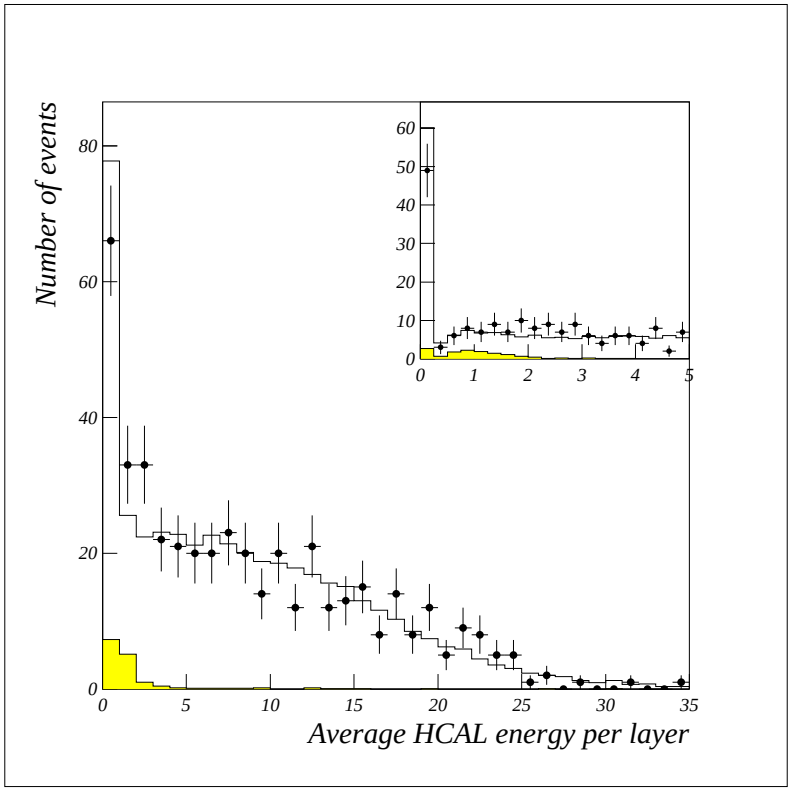

Figure 5: The distribution of average HCAL energy per layer for selected tau hadronic decays. The anti-muon selection cut rejects the region between 0.5 and 1.5 GeV.

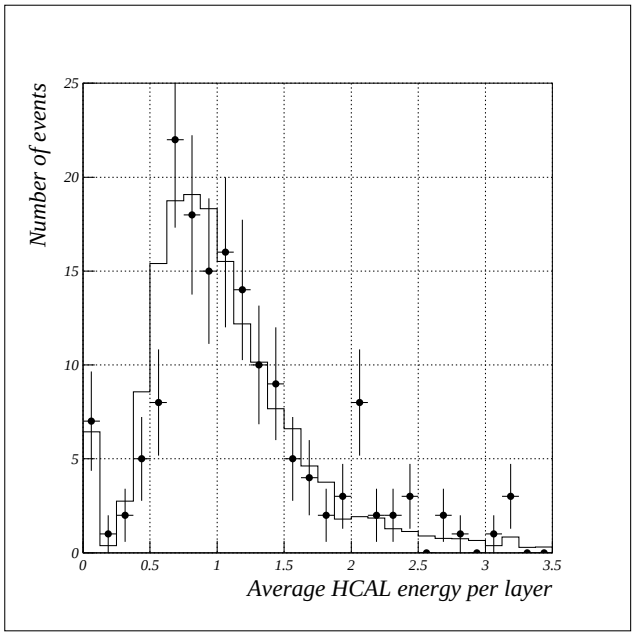

Figure 6: The distribution of average HCAL energy per layer for a test sample of tau decays to muons. Points are data and histogram is simulation.

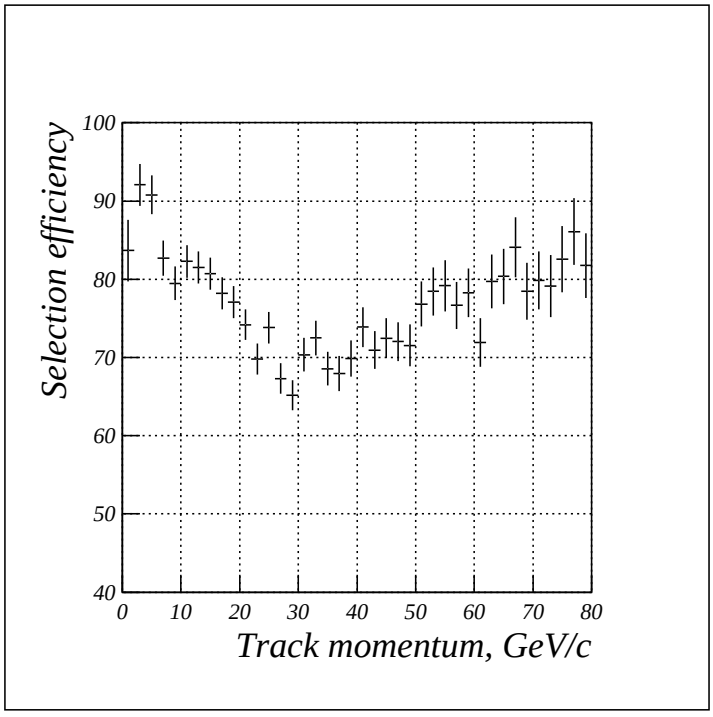

Figure 7: Tau hadronic decay selection efficiency as a function of leading track momentum. The efficiency has been estimated from simulation.

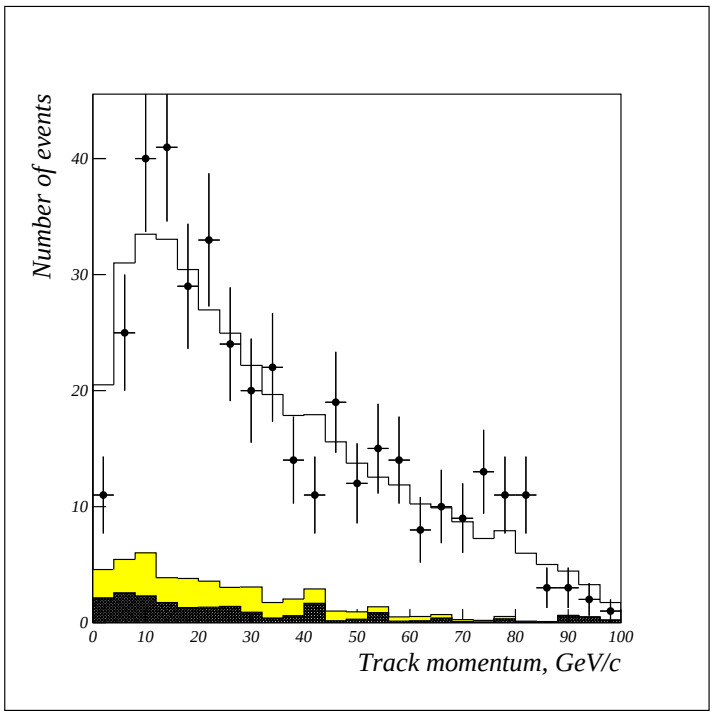

Figure 8: The distribution of track momentum for the selected tau hadronic decays.

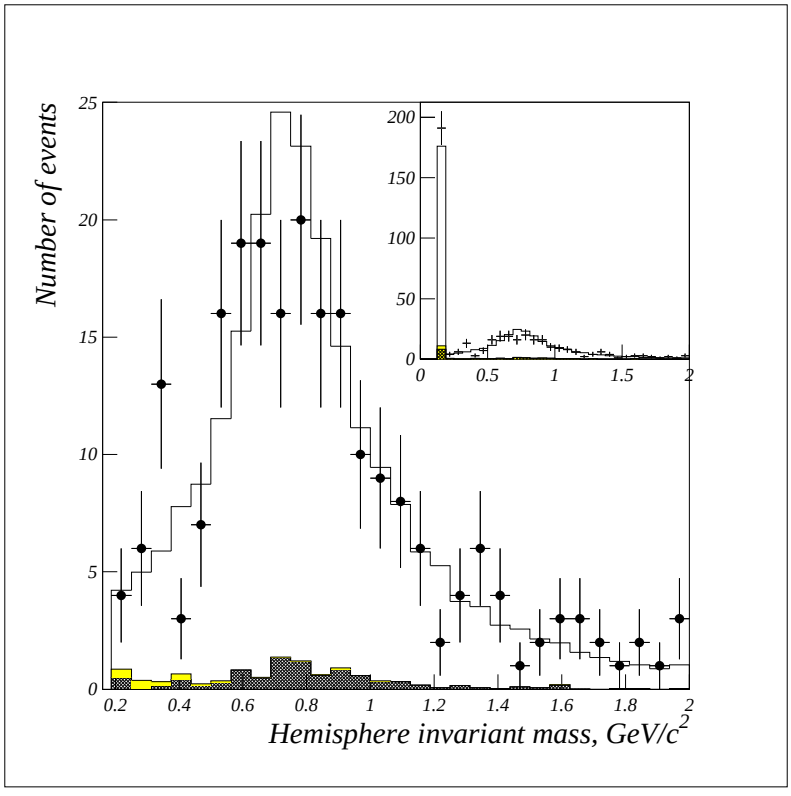

Figure 9: Reconstructed invariant mass of tau hadronic decay products. The inset shows the same histogram together with the first bin corresponding to no photons detected. The points are data, the solid line is simulation, the black and gray histograms are external and internal background.

In this analysis the chosen observables sensitive to polarisation were two angles, θ and ψ which characterise decays of the tau and of the daughter hadronic resonance. They were defined as follows:

$$cos\theta = \frac{2p_h/p_\tau - 1 - m_h^2/m_\tau^2}{1 - m_h^2/m_\tau^2}, \qquad cos\psi = \frac{E_{ch} - E_{neu}}{E_{ch} + E_{neu}}, \tag{1}$$

where p_h and m_h are the reconstructed momentum and invariant mass of the hadronic system, and E_{ch} and E_{neu} are the total energies of charged and neutral products of tau decay. More details can be found in [1].

The polarisation was extracted by fitting the real data distribution of sensitive variable by the Monte-Carlo expectation f_{MC} with tau polarisation P_τ as a free parameter:

$$f_{MC} = f_{bg} + R \cdot \left(\frac{1 - P_\tau}{1 - P_0} f_L + \frac{1 + P_\tau}{1 + P_0} f_R \right), \tag{2}$$

where f_{bg}, f_L and f_R are the contributions from external background and from taus with negative and positive helicity, and P_0 is the generator level tau polarisation in the simulated tau pair events. The external background contribution was normalised to luminosity. The factor R normalises the number of events in the simulated tau signal to the real data after external background subtraction:

$$R \cdot N_{\tau\tau-MC} = N_{data} - N_{bg} \tag{3}$$

Such a fit automatically takes into account a bias due to different selection efficiency for different tau helicity. It also does not depend on the tau polarisation in the simulated tau pair sample.

The tau polarisation was extracted separately for each of the three years. The two-dimensional distributions of $cos\theta$ versus $cos\psi$ were fitted simultaneously in the three bins of the invariant mass. For the first bin of invariant mass only one-dimensional distribution of $cos\theta$ was used because this bin is dominated by decays to pions and so ψ is meaningless. The results of the fit are presented in Table 1. The corrections described in the next section are not applied to these values. As a cross-check the fit was also performed for a single data sample with all three years combined. The Monte-Carlo samples were added with weight proportional to luminosity. The result of this fit was very close to the average of year-by-year results.

Year	τ polarisation	stat. error
1997	-0.07	0.24
1998	-0.37	0.21
1999	-0.10	0.20

Table 1: Results of tau polarisation fit to each year data.

The results of the fit are illustrated in Fig. 10 which shows the distribution of $cos\theta$ for the first bin of invariant mass and one-dimensional projections of the fitted two-dimensional distributions for other invariant masses. Combined data of all years are shown and the simulated signal is shown with the tau polarisation obtained from the fit.

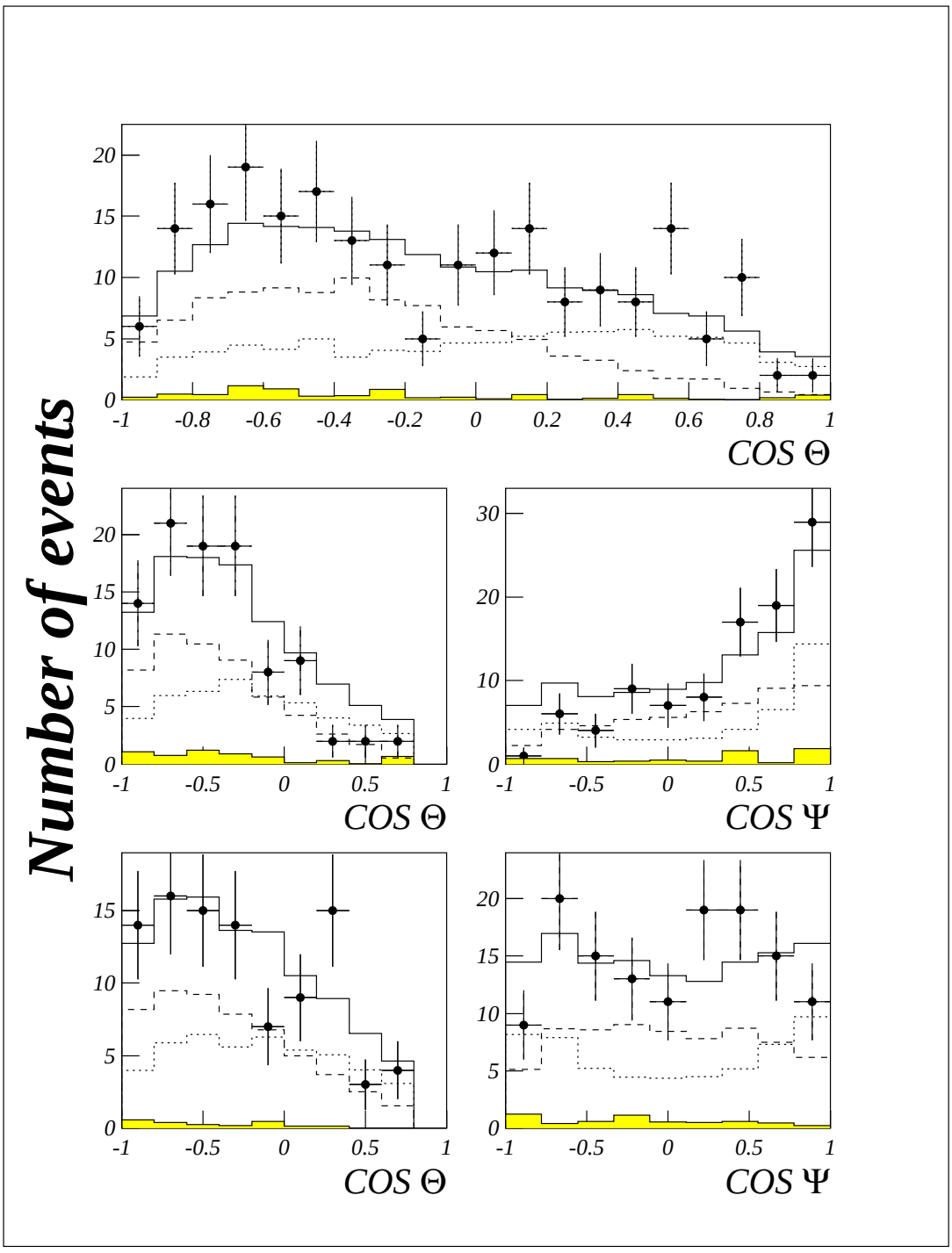

Figure 10: The distributions used in the fit to tau polarisation for the first bin of invariant mass (upper), second (middle) and third bin of invariant mass (lower). Points represent data, solid lines represent simulated signal and grey histograms represent external background. Dashed (dotted) lines represent contributions of tau with negative (positive) helicity.

4 Systematic errors

Since this analysis strongly relies on the Monte-Carlo distributions used in the fits, the main sources of systematic errors are due to a possible disagreement between data and Monte-Carlo. When possible the selection efficiency was estimated from the data itself using test samples and the agreement with Monte-Carlo was checked. The precision of these comparisons was limited by the statistics of the test samples which was translated into uncertainty on tau polarisation.

Some of such comparisons have led to corrections which were then applied to the results of the fits described in previous section. In these cases the uncertainty of the correction was added to the total systematic error.

For example, the redundancy between cuts on HPC and HCAL energies (see Fig.3) allows one to estimate from the data itself the momentum-dependent selection efficiency for each detector using events selected by another detector as a test sample. The efficiency of the "OR" of the two cuts was then compared with the Monte-Carlo values and the small discrepancy was propagated to a correction to the tau polarisation. The uncertainty of the efficiency determination was propagated to the systematic error on the tau polarisation. Similarly, the redundancy between the hadron calorimeter and the muon chambers was used to estimate the efficiency of muon rejection cuts.

In the cases when the measurement of selection efficiency directly from data was not possible and the analysis relied only on Monte-Carlo the systematic errors were estimated from variation of selection cuts typically by a value of resolution of the corresponding variable.

The systematic uncertainties on tau polarisation are summarised in table 2 and the correction which have to be applied to the tau polarisation are summarised in table 3. It should be noted that the systematic error and the corrections are common to the results of all three years. In most cases they were estimated using test samples selected from all available data to increase statistics.

5 Summary

Averaging the tau polarisation values obtained from the fits to data from individual years and applying the corrections described in previous section one gets the result:

$$P_\tau = -0.16 \pm 0.13 \pm 0.05, \tag{4}$$

where the first error is statistical and the second is systematic. The systematic error of the measurement has predominantly statistical origin and it can be reduced if the data of 2000 is added.

Fig. 11 shows the Standard model prediction of tau polarisation versus collision energy. Superimposed are the measurements performed using the inclusive selection of one-prong hadronic tau decays. The two points correspond to LEP1 and LEP2 data.

Source	$\Delta P_\tau, 10^{-3}$
"HPC or HCAL" efficiency	25
Monte-Carlo statistics	21
M_{INV} binning	20
HPC γ efficiency	18
dE/dx momentum dependence	15
dE/dx absolute calibration	13
HCAL energy per layer	12
Internal background $\pm 20\%$	12
E_γ scale	10
HCAL energy beyond 1st layer	7
HPC associated energy scale	6
External background $\pm 30\%$	5
Contamination from $\sqrt{s'/s} < 0.9$	5
$\mathrm{Br}(\tau \to \pi\nu)$	5
Total	52

Table 2: Summary of systematic uncertainties on tau polarisation.

Source	$\Delta P_\tau, 10^{-3}$
"HPC or HCAL" efficiency	+16
HPC gamma efficiency	+7
$\mathrm{Br}(\tau \to \pi\nu)$	+5
Total	+28

Table 3: Corrections to be applied to the tau polarisation.

References

[1] DELPHI coll., Zeit. Phys. C67 (1995) 183
DELPHI coll., E. Phys. J. C14 (2000) 585

[2] DELPHI coll., Eur. Phys. J. C11 (1999) 383
DELPHI coll., Phys.Lett. B485 (2000) 45

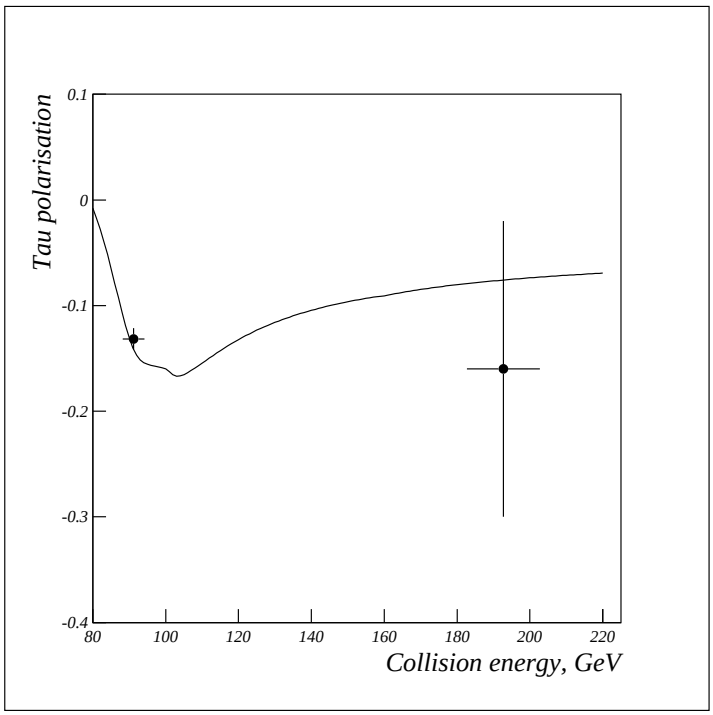

Figure 11: Tau polarisation versus collision energy: Zfitter prediction (curve) and DELPHI measurements using one-prong hadronic decays (points). Horizontal bars show ranges of LEP energies used in each measurement. All the polarisation values are given assuming the cut $\sqrt{s'} < 0.9\sqrt{s}$.